Nanoconfinement Revealed in Degradation and Relaxation Studies of Two Structurally Different Polystyrene−Clay Systems

Kai Chen,[†] Charles A. Wilkie,[‡] and Sergey Vyazovkin*[,†]

Department of Chemistry, University of Alabama at Birmingham, 901 S. 14th Street, Birmingham, Alabama 35294, and Department of Chemistry, Marquette University, P.O. Box 1881, Milwaukee, Wisconsin 53201

Received: July 26, 2007; In Final Form: September 11, 2007

Degradation and relaxation studies have been performed on two polystyrene (PS)−montmorillonite clay nanocomposites, one of which has an intercalated PS−clay structure and the other an exfoliated PS−clay brush structure. Compared to virgin PS, both nanostructured materials have demonstrated the following similarities: (a) a high yield of α-methylstyrene in the degradation products as measured by infrared spectroscopy; (b) larger values of the activation energy of the thermal degradation as determined by isoconversional kinetic analysis of thermogravimetric data; and (c) larger values of the activation energy for the glass transition as found from the frequency dependence of the glass transition temperature measured by multifrequency temperature-modulated differential scanning calorimetry. These effects are taken as structure independent manifestations of nanoconfinement of the PS chains in the PS−clay materials. Heat capacity measurements have been employed to evaluate the size of the cooperatively rearranging region, V_{CRR}, that is found to be structure dependent. Compared to its value in virgin PS, V_{CRR} has markedly increased in the exfoliated PS−clay brush system but remained practically unchanged in the intercalated PS−clay system.

Introduction

Dispersion of layered silicates into a polymer matrix results in the formation of intercalated and/or exfoliated nanostructures that can dramatically change the thermal behavior[1−6] of the resulting polymer−clay nanocomposites. Compared to virgin polymers, a remarkable increase in the thermal decomposition temperature as well as the glass transition temperature (T_g) of the polymer−clay nanocomposites broadens their potential application area. A substantial reduction in the peak heat release rate determined by cone calorimetry suggests that nanocomposites can be beneficial for reducing the flammability of materials. In order to transfer these highly desirable properties into commercial success, it is crucial to understand the mechanism of the thermal property enhancement in the polymer−clay nanocomposites. As one of the commonly invoked mechanisms, the barrier model[7,8] suggests that a silicate-enriched char layer builds up on the polymer melt surface and provides the mass and heat transfer barrier. An increase in the concentration of silicates at the polymer melt surface has been detected experimentally[9] and explained theoretically.[10] It has also been reported that the catalytic activity of nanodispersed silicate clay can change the condensed phase decomposition behavior and promote the char formation for certain polymers, such as polyethylene[11] and polypropylene,[12] which normally are non-char-forming polymers. The increased residual char helps to insulate the underlying polymer and slows its mass loss due to the thermal decomposition. However, some polymer nanocomposites have too small a loading of clay (i.e., 0.1% by weight) to be able to form efficient protective layers. A radical trapping model[13] has been proposed to emphasize that the structural iron in the clay can trap the polymeric radicals and slow the degradation process in the nanocomposites having a very low loading of clay.

Although the barrier and radical trapping models provide important insights into the thermal behavior of polymer−clay nanocomposites, the fundamental effects of silicate clay on the observed thermal property enhancements are not yet well understood. It is commonly believed that the exfoliated clay structures generate a more uniform phase mixing and thus a larger contact area between the clay phase and polymer matrix which should result in stronger property enhancement than in the case of the intercalated structures. However, the measured thermal properties based on a wide range of polymer−clay nanocomposites do not show consistent results. While many polymer nanocomposites exhibit an increased T_g as a signature of improved thermal stability due to the restricted segmental motions,[14−16] a decrease of T_g is also found in both intercalated and exfoliated nanocomposites.[17−19] A recent study on polystyrene−clay nanocomposites[20] with various clay types, concentrations, and extents of clay dispersion concludes that changes in the glass transition temperatures of the nanocomposites do not correlate with whether the clay structure is intercalated or exfoliated. In addition, some thermogravimetric analysis (TGA) measurements[7] and molecular dynamics simulations[21] indicate that intercalated nanocomposites are more thermally stable than exfoliated nanocomposites. This unexpected result suggests that the thermal stability of polymer−clay nanocomposites cannot be explicitly explained by the dispersion state of the clay. Other factors, such as the chemical nature of the nanocomposite components and preparation and processing methods, appear to be involved in the complex structure−property relationship. The current nanocomposite studies are mostly phenomenological so that the actual molecular origins of thermal stability remain far from being well understood. On the other hand, designing of polymer−clay nano-

* To whom correspondence should be addressed. E-mail: vyazovkin@uab.edu.
[†] University of Alabama at Birmingham.
[‡] Marquette University.

10.1021/jp0759168 CCC: $37.00
Published on Web 10/18/2007

composites with desired thermal properties would require finding at least semiquantitative structure−property relationships.

The effect of silicate clay on the properties of polymer nanocomposites is undoubtedly associated with the fact that the dispersed clay platelets have a nanoscopic size (<100 nm), comparable to the typical size of a polymer chain estimated as the radius of gyration, R_g, that is typically on the order of 5−20 nm.[22] The nanoscale dimensions and spatial arrangements of clay particles create the locally confined environments (so-called nanoconfinement) for polymer chains that cannot be accomplished in the bulk polymers or conventional polymer composites with microscale fillers. For example, the extremely narrow spacing (1−5 nm) in the gallery of the intercalated clay structure is much smaller than R_g so that the formation of the regular coil conformation typical of the neat bulk polymer is not possible. As a result, the conformations and segmental motion of intercalated polymer chains are dramatically different from those in the bulk.[23] The nanoscopic dimensions of silicate layers give rise to an enormously high interfacial area between the polymer chains and clay platelets. Complete exfoliation of layered silicates can generate a specific surface area of 750 m^2/g,[24] while the traditional particulate fillers normally have a surface area of 3−5 m^2/g.[25] Even at low clay loadings, the nanocomposites may have a very large interfacial region where the polymer chains can be nanoconfined and their dynamics altered compared to the bulk. Therefore, nanoconfinement can be revealed by studying the processes closely related to the chain dynamics, such as relaxation and degradation. Furthermore, evaluating the physical parameters of these processes can provide a way of evaluating nanoconfinement.

Recent efforts of Vyazovkin's group have been focused on comprehensively studying an exfoliated PS−clay brush system, the structure of which has been discussed in detail elsewhere.[26,27] The group has studied the kinetics of degradation[28] and relaxation (glass transition)[29,30] as well as the degradation mechanism[26,27] of this system as compared to virgin PS. The relaxation studies[29,30] have shown that compared to virgin PS, the PS−clay material has a significantly larger value of both activation energy and the cooperatively rearranging region of the glass transition. An increase in both parameters has been taken as evidence of nanoconfinement resulting from the formation of the brush structure. On the other hand, the degradation studies[28,29] have demonstrated that compared to virgin PS, the PS−clay system has a markedly larger activation energy and smaller heat of thermal degradation. The change in the thermal effect has hinted at a possible alteration of the degradation mechanism. Further spectroscopic studies[26] of degradation products have detected abnormally high yields of α-methylstyrene in addition to styrene monomer, dimer, and trimer typically observed in degradation of virgin PS.[31−33] Because α-methylstyrene is a product of interchain hydrogen transfer, its formation is readily explained by nanoconfinement of PS chains estimated as a decrease in the average interchain distance from 8.2 nm in virgin PS to 3.8 nm in the PS−clay brush system.[26] Nanoconfinement has thus been put forward as a key factor that can alter the chemical behavior of the confined polymer chains. However, an abnormally high yield of α-methylstyrene has been also reported by Jang and Wilkie[34] in an independent degradation study of an intercalated PS−clay material. Although Jang and Wilkie have explained the result by the barrier effect of clay, their notion of the "barrier" is not limited to a silicate-enriched char layer formed on the polymer melt surface, but rather it covers the general situation when clay exerts spatial constraints on a polymer and its degradation products. In this meaning, the notion of the "barrier" is conceptually identical to the notion of "nanoconfinement" used in the present paper.

The structure of the intercalated PS−clay material is much more complex than that of the exfoliated PS−clay brush system so that the respective nanoconfinement cannot be estimated directly from the dimensions of intercalated clay particles. The concurrence of the mechanistic patterns of degradation in these two systems suggests that they both may exert similar nanoconfinement on the PS chains. Because the previous studies of the exfoliated PS−clay brush system have demonstrated that nanoconfinement reveals itself in the kinetics of degradation as well as of relaxation, the present study continues to explore the kinetics of these processes in the aforementioned intercalated PS−clay material. In addition to collecting comparative kinetic information on the two chemically similar materials of different morphological structures, the present study attempts to identify which of the aforementioned parameters (i.e., the activation energies of degradation and relaxation, and the size of cooperatively rearranging region) are generally relevant for revealing and evaluating nanoconfinement. Also, the paper reports new results of the relaxation measurements performed on the intercalated PS−clay material as well as on the exfoliated PS−clay brush system and on virgin PS by using the novel technique[35] of multifrequency temperature-modulated differential scanning calorimetry (DSC).

Experimental Section

Preparation and characterization of the PS−montmorillonite (MMT) clay nanocomposites used in this study have been described in detail elsewhere.[36−38] Briefly, the intercalated PS−clay sample was prepared at Marquette University by a bulk polymerization technique.[36] The organically modified MMT clay (under commercial name Cloisite 10A, containing a surfactant of dimethylbenzyl hydrogenated tallow ammonium chloride) was used as received from Southern Clay Product Inc. A radical initiator azobis(isobutyronitrile) (AIBN) and styrene monomer were mixed with the organically modified MMT by stirring at room temperature under flowing nitrogen gas. The bulk polymerization was carried out at 60 °C for 24 h and then at 80 °C for 24 h. The intercalated structure of the resulting nanocomposites was confirmed by X-ray diffraction (XRD)[34,36] and transmission electron microscopy (TEM)[13] for the samples with clay contents from 1% to 5% by weight. The exfoliated PS−clay nanocomposite containing 1% by weight of MMT was prepared at the University of Alabama at Birmingham by a solution surface-initiated polymerization (SIP) method.[37,38] A monocationic initiator (AIBN−analogue compound with quaternized amine group at one end) was intercalated inside the gallery of pristine MMT via cation exchange reaction in which the cationic end of the initiator was ionically attached to the negatively charged silicate surface.[37] The initiator-modified clay particles were mixed with styrene monomer in THF solvent. At 60 °C, the in situ polymerization under nitrogen atmosphere was directly initiated from the clay surface[38] to which the initiators have been attached. In the final products, the exfoliation of MMT clay and the attachment of the initiator and PS chains onto the clay surface were demonstrated[37,38] by XRD, infrared spectroscopy (IR), X-ray photoelectron spectroscopy (XPS), and atomic force microscopy (AFM). For comparison purposes, radically polymerized neat PS (Alfa Aesar) was used as received.

M_w of the intercalated nanocomposites has been measured by using size exclusion chromatography and PS standards and

was found to be 1.76×10^5, 1.26×10^5, and 1.61×10^5 g mol^{-1} for the systems with 1%, 3%, and 5% clay load, respectively. The M_w values are comparable to the previously determined values for the exfoliated system (0.90×10^5 g mol^{-1}) and for virgin PS (1.00×10^5 g mol^{-1}).[29]

The degradation kinetics have been measured as the temperature-dependent mass loss using thermogravimetric analysis (Mettler-Toledo TGA/SDTA851^e). Samples of ~10 mg have been heated in the flowing atmosphere of N_2 at a flow rate of 70 mL min^{-1} from 25 to 600 °C at the heating rates of 2.5, 5.0, 7.5, 10.0, and 12.5 °C min^{-1}. The buoyancy effect in TGA has been accounted for by performing empty pan runs and subtracting the resulting data from the subsequent sample mass measurements.

The degradation products have been analyzed in situ by infrared spectroscopy (Nicolet Nexus 470 FTIR coupled with Mettler-Toledo TGA/SDTA851^e). The heating rate was 10 °C min^{-1}, and FTIR spectra were collected at 4 cm^{-1} resolution.

The glass transition (relaxation) kinetics have been determined by multifrequency temperature-modulated DSC (TOPEM DSC 823^e by Mettler Toledo). For brevity purposes, the technique is called "multifrequency DSC" throughout the rest of the paper. By overlaying a series of stochastic temperature pulses of different duration with a temperature ramp at a constant underlying rate, one single multifrequency DSC measurement allows one to determine the frequency dependence of the complex heat capacity that can be conveniently used to characterize the glass transition dynamics. Samples of ~5 mg were isothermally held at the temperature of ~40 °C above the glass transition temperature for 10 min to erase the thermal history. Then the glass transition was measured on cooling to a temperature of ~40 °C below the T_g. The temperature program for all measurements was defined by superimposing the underlying cooling rate of 0.5 °C min^{-1} and a series of stochastic temperature pulses of the 1 °C amplitude with the time between the pulses ranging from 25 to 60 s. DSC has been calibrated using indium and zinc standards. All the degradation and relaxation studies have been conducted at the University of Alabama at Birmingham.

Analysis of the Degradation Kinetics. Polymer degradation is a complex process that may involve multiple simultaneously occurring steps, such as random or end-chain scission, chain transfer, recombination, etc. For this reason, it can rarely be described by a single-step rate equation[39]

$$\frac{d\alpha}{dt} = A \exp\left(\frac{-E}{RT}\right) f(\alpha) \tag{1}$$

that would hold throughout the whole range of the degradation temperatures and conversions. In eq 1, α is the extent of polymer conversion, t is the time, T is the temperature, R is the gas constant, A is the pre-exponential factor, E is the activation energy, and $f(\alpha)$ is the reaction model. As shown recently,[40] the use of a model-free isoconversional method provides a very effective approach to handling complex kinetics in polymer systems. The basic assumption of the isoconversional methods is that the reaction model is independent of temperature or heating rate. Then, at a constant extent of conversion, the reaction rate is only a function of the temperature:

$$\left[\frac{d \ln(d\alpha/dt)}{dT^{-1}}\right]_\alpha = -\frac{E_\alpha}{R} \tag{2}$$

Although eq 2 is derived from the single-step rate eq 1, E_α is assumed to be a constant only for a given extent of conversion and the narrow temperature region related to this conversion. In other words, the isoconversional methods describe the degradation kinetics by using eq 1 multiple times, each of which is associated with a certain extent of conversion and has its own value of E_α. The resulting value has a meaning of the effective activation energy, and its variation with α and T can provide important insights into the mechanism and kinetics of complex processes.[40]

The present study makes use of an advanced isoconversional method developed by Vyazovkin.[41,42] The method offers two major advantages over the frequently used methods of Flynn and Wall[43] and Ozawa.[44] The first advantage is that it has been designed to treat the kinetics that occur under arbitrary variation in temperature, $T(t)$, which allows one to account for self-heating/cooling detectable by the thermal sensor of the instrument. For a series of n experiments carried out under different temperature programs, $T_i(t)$, the activation energy is determined at any particular value of α by finding E_α, which minimizes the function[41,42]

$$\Phi(E_\alpha) = \sum_{i=1}^{n} \sum_{j \neq i}^{n} \frac{J[E_\alpha, T_i(t_\alpha)]}{J[E_\alpha, T_j(t_\alpha)]} \tag{3}$$

where

$$J[E_\alpha, T_i(t_\alpha)] \equiv \int_{t_{\alpha-\Delta\alpha}}^{t_\alpha} \exp\left[\frac{-E_\alpha}{RT_i(t)}\right] dt \tag{4}$$

The second advantage is associated with performing integration over small time segments (eq 4) that allows for eliminating a systematic error[42] occurring in the Flynn and Wall and Ozawa methods when E_α varies significantly with α. In eq 4, α is varied from $\Delta\alpha$ to $1 - \Delta\alpha$ with a step $\Delta\alpha = m^{-1}$, where m is the number of intervals chosen for analysis. The integral, J in eq 3, is evaluated numerically by using the trapezoid rule. The minimization procedure is repeated for each value of α to find the dependence E_α on α.

Analysis of the Glass Transition Dynamics. During the glass transition an amorphous polymer relaxes from the nonequilibrium glassy state toward the equilibrium liquid state. The relaxation rate is described by a first-order kinetic equation[45]

$$\frac{d\xi}{dt} = -\frac{1}{\tau}(\xi - \xi_e) \tag{5}$$

where ξ and ξ_e are, respectively, the nonequilibrium and equilibrium values of an order parameter such as enthalpy, and τ is the relaxation time. The temperature dependence of τ can be introduced via the Arrhenius equation

$$\tau = A \exp\left[\frac{E}{RT}\right] \tag{6}$$

The activation energy of the relaxation process can be determined from the frequency dependence of the glass transition temperature. The multifrequency DSC technique measures the glass transition at different frequencies as a stepwise change in the heat capacity, the midpoint of which can serve as an estimate of T_g. The resulting value of T_g increases with the frequency, f. Due to the reciprocal relation between f and τ, eq 6 allows one to calculate the activation energy of the glass transition from eq 7

$$E = -R\frac{d \ln f}{dT_g^{-1}} \tag{7}$$

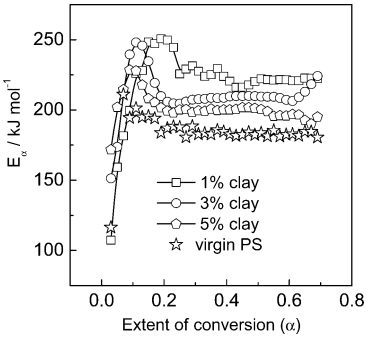

Figure 1. Dependence of the activation energy (E_α) of degradation on the extent of conversion.

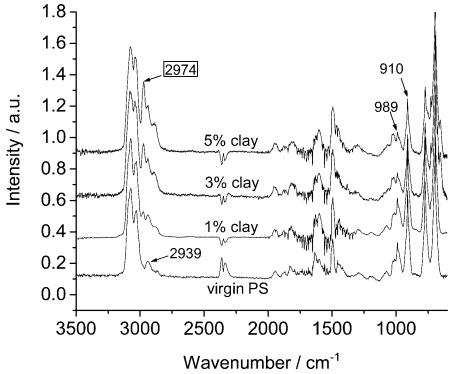

Figure 2. Gas phase IR spectra of degradation products.

The advantage of the multifrequency technique is that the evaluation of the activation energy is accomplished in a single experiment, eliminating run-to-run experimental errors unavoidable when using a series of single-frequency runs in regular temperature-modulated DSC as well as a series of single heating rate runs in regular DSC to determine the activation energy.[46]

The glass transition dynamics has a cooperative nature. In order to test the effect of nanoconfinement on the intermolecular cooperativity of the PS matrix, the size of cooperatively rearranging region (CRR) has been estimated from the data on the quasi-static heat capacity, $C_{p,0}$. The latter is obtained from the multifrequency DSC measurements as the reversing heat capacity corresponding to the zero frequency. The data analysis is based on Donth's equation:[47,48]

$$V_{CRR} = \frac{k_B T_g^2 \Delta(C_v^{-1})}{\rho(\delta T)^2} \tag{8}$$

where V_{CRR} is the volume of CRR, k_B is the Boltzmann constant, T_g is an apparent glass transition temperature defined as the midpoint of the step change in $C_{p,0}$, ρ is the density (1.05 g cm^{-3} for PS[49]), and C_v is the isochoric heat capacity. The value of $\Delta(C_v^{-1})$ is determined as

$$\Delta(C_v^{-1}) = C_{vg}^{-1} - C_{vl}^{-1} \tag{9}$$

where C_{vg} and C_{vl} are the respective values of the glassy and liquid heat capacity extrapolated to T_g. The difference between isochoric and isobaric heat capacities can be accounted for via the following correction:[50]

$$\Delta(C_v^{-1}) = (0.74 \pm 0.22)\Delta C_p^{-1} \tag{10}$$

For the glass transition measured on cooling, the mean temperature fluctuation, δT, is estimated as

$$\delta T = \frac{\Delta T}{4} \tag{11}$$

where ΔT is the temperature interval within which C_p varies between 16% and 84% of the total ΔC_p step at T_g.[50]

Results and Discussion

Degradation. Figure 1 displays the results of the isoconversional kinetic analysis for the thermal degradation of the intercalated PS−clay nanocomposites and virgin PS in the atmosphere of N_2. Regardless of the clay content, the degradation process of the intercalated nanocomposites shows a larger effective activation energy as compared to that of virgin PS. An increase in E_α of degradation is likely to be responsible for the enhanced thermal stability of the intercalated PS−clay material. In a previous study[29] on the exfoliated PS−clay brush system, it has also been observed that the activation energy for the degradation of the brush system is markedly larger than for virgin PS. Similar effects have later been reported by other workers for the degradation of nanocomposites of polyethylene,[51] poly(methyl methacrylate),[52] and polyamide.[53]

An increase in the activation energy of degradation is difficult to rationalize in terms of the formation of the surface silicate barrier which can delay the diffusion of gaseous decomposition products and slow the degradation process as suggested by the barrier model. Because diffusion of gases in liquids and solids, including polymers, tends to have a low activation energy of about 40−50 kJ mol^{-1},[54] the formation of a diffusion barrier should decrease the effective value of E_α. More importantly, Figure 1 further shows that the variation of E_α for all intercalated PS nanocomposites displays a ∼30−50 kJ mol^{-1} peak in E_α at the early stages of degradation (extent of conversion, $\alpha < 0.2$). This indicates that the presence of clay has a stronger stabilizing effect on the PS in the early stages. This phenomenon also does not seem consistent with the barrier model. It has been observed[55] that the surface barrier grows throughout the degradation process of nanocomposites as the clay platelets migrate to and reassemble at the surface. Therefore, from the standpoint of the barrier model, one should rather expect a stronger stabilizing effect at later degradation stages. However, the peak in E_α plots can be explained by assuming that, in the nanoconfined environment, diffusion of degrading radicals slows to the point that they can recombine, making degradation partially reversible. As the degradation progresses toward larger extents of conversion and higher temperatures, nanoconfinement disintegrates and recombination of the degrading radicals becomes unlikely, turning degradation into a regular irreversible mode. That is, the overall process of PS radical degradation appears to proceed via a reversible degradation step, which takes place in the nanoconfined environment and which is followed by an irreversible degradation step that occurs after the nanoconfined environment has disintegrated. For a process proceeding via an endothermic reversible step followed by an irreversible step, the initial stages are known[42,56] to demonstrate a markedly larger effective activation energy, whose value is determined by the sum of the enthalpy of the reversible step and the activation energy of the irreversible step. On the other hand, the later stages of such a process yield[42,56] an effective activation energy, whose value approaches the activation energy of the irreversible step.

In order to obtain further insights into the effect of clay on the various stages of degradation of the PS nanocomposites, the evolution of degradation products has been analyzed by

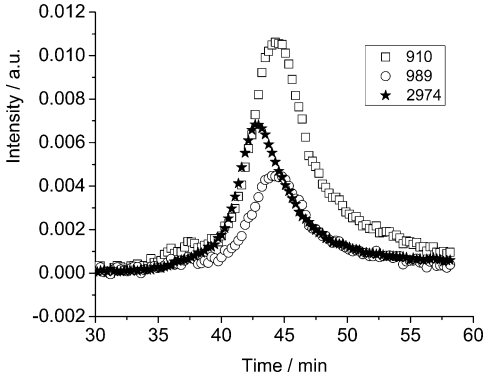

Figure 3. Evolution of IR absorption bands at 910, 989, and 2974 cm^{-1} in degradation products of intercalated PS−clay (5% of clay) nanocomposite.

using a FTIR spectrometer coupled with TGA. Figure 2 shows that the degradation of the intercalated PS−clay sample demonstrates distinct absorption at 2974 cm^{-1} that is especially strong in the sample with a higher clay content. This absorption is undetectable in the degradation products of virgin PS. It has been found[26,34] that the absorption at 2974 cm^{-1} is associated with the methyl stretch of α-methylstyrene. Therefore, two conclusions can be drawn here: first, significant amounts of α-methylstyrene indicate that the degradation pathway of intercalated PS−clay is different from that of virgin PS, which yields only trace amounts of this product; second, the yield of α-methylstyrene increases with an increase of the clay content in the nanocomposites.

Figure 3 compares the evolution of two degradation products, styrene monomer and α-methylstyrene, from the intercalated nanocomposite (5% of clay) by monitoring their respective absorption bands at 910 and 989 cm^{-1} (out-of-plane ═C−H bending of the vinyl group in styrene) as well as at 2974 cm^{-1} (C−H stretching of methyl in α-methylstyrene). The evolution of these bands as a function of degradation time (Figure 3) clearly shows that for the intercalated PS−clay composite the trace of α-methylstyrene (2974 cm^{-1}) reaches its maximum faster than the trace of styrene (910 and 989 cm^{-1}). Note that a similar effect has already been reported[26,27] for degradation of the exfoliated brush system. The intercalated nanocomposites with lower clay loadings (1 and 3%) show the same trend with the only difference being that the relative intensity of α-methylstyrene evolution becomes smaller as the clay loading decreases. The observed trend suggests that α-methylstyrene is produced predominantly in the early stages of degradation. In other words, the degradation of PS in the intercalated nanocomposite changes its pathway as degradation progresses to a higher extent of conversion. The change in the pathway appears to correlate with the variation in E_α data (Figure 1). That is, at low extent of conversion, the degradation of intercalated PS produces more α-methylstyrene and a peak in the E_α-dependence is observed. It is noted that a similar correlation between the evolution of α-methylstyrene and the variation of E_α has been observed for the exfoliated PS−clay brush material in the previous study.[26,27] Since these two PS−clay systems have very different nanoscale structures, the question arises whether there can be a common reason that causes the degradation pathway to change in a similar way.

In order to answer this question, one needs to recall that the formation of α-methylstyrene is a result of interchain hydrogen transfer, so that it can be intensified by decreasing the interchain distance due to nanoconfinement in the brush structures. The decrease is easy to visualize and evaluate in the exfoliated PS−clay brush material. However, this is not the only way in which the clay phase can introduce nanoconfinement into the polymer matrix. Extensive morphological studies[57−60] have demonstrated that the characteristic length of dispersed clay particles varies over a wide range down to a few nanometers that is much smaller than a typical diameter of unperturbed polymer coils. Therefore, the hierarchical structures of the clay particles dispersed in the polymer matrix are likely to create various locally confined environments in which polymer chains cannot maintain their regular coil conformation. In addition, many polymer chains, or their segments, are located in the interfacial region close to the clay platelets. A number of simulation studies[61−64] have shown that the polymer chains near the solid surface (e.g., silicate clay) are flattened, and their shape is quite different from the regular coil conformation. The calculated local density of polymer chains displays a characteristic oscillatory behavior as a function of distance from the solid surface, so that there are alternating layers whose respective densities are smaller and larger than the bulk density. Although the magnitude and persistent distance of density oscillation depends on the strength of interfacial interaction, the shape of solid surface, and the model chosen for the simulation, the upshot is that the polymer chains in the nanocomposites can experience nanoconfinement at least near the clay surface.

The above types of nanoconfinement as well as nanoconfinement inside the clay galleries can readily occur in the intercalated PS−clay material. The nanoconfined environments put PS chains in a crowded situation therefore reducing the interchain distance, as in the case of exfoliated PS−clay brush material. As a result, the polymer chains are likely to engage in the interchain hydrogen transfer to yield α-methylstyrene. The more intercalated clay particles in the system, the larger the interfacial area, and more PS chains experience nanoconfinement. This is obviously consistent with the observation (Figure 2) that the intercalated PS−clay system with 5% of clay produces more α-methylstyrene than the system with 1% of clay. Also at the early stages of degradation in both intercalated and exfoliated PS−clay systems, most nanoconfined structures of dispersed clay remain preserved but become gradually destroyed as the extent of degradation increases. Consequently, there is a stronger nanoconfinement and larger degree of stabilization of polymer chains at the early stages of degradation. This is reflected in the effective activation energy peak, whose maximum is observed at $\alpha < 0.2$ (Figure 1).

Relaxation. As mentioned earlier, nanoconfinement can distort dramatically the conformation of the polymer coils. In particular, the aforementioned decrease in the interchain distance should enhance intermolecular interaction and, thus, hinder molecular mobility. For this reason, nanoconfinement should be expected to reveal itself in the glass transition dynamics of the polymer nanocomposites.

The glass transition dynamics have been characterized in terms of a size of a cooperatively rearranging region and an activation energy of the glass transition. These two quantities can be determined by measuring the heat capacity in the glass transition region by using multifrequency DSC. An example of a multifrequency DSC measurement is given in Figure 4. The real part of the complex heat capacity is evaluated at the frequencies, f, from 5 to 35 mHz, and $C_{p,0}$ is the quasi-static heat capacity at the zero frequency.

The activation energy of the glass transition has been evaluated from the frequency dependence of T_g (eq 7) determined in multifrequency DSC measurements. The values of E

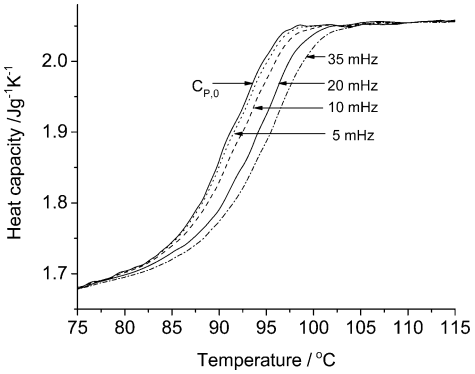

Figure 4. Frequency dependence of the heat capacity for virgin PS evaluated by multifrequency DSC. ($C_{p,0}$ is the quasi-static heat capacity when frequency approaches zero.)

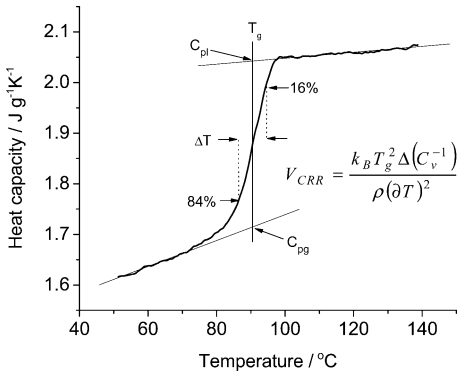

Figure 6. Evaluating the size of the cooperatively rearranging region (V_{CRR}) from the quasi-static heat capacity ($C_{p,0}$) curve for virgin PS.

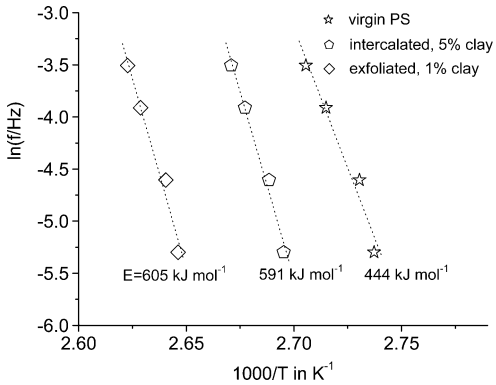

Figure 5. Activation energies of the glass transition determined from frequency dependence of heat capacity. (The reported E is an averaged value based on at least three measurements.)

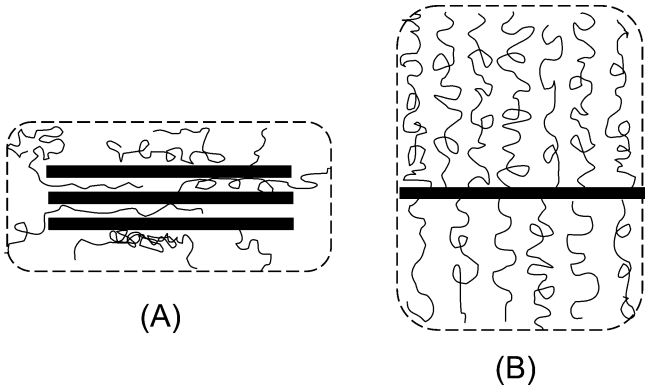

Figure 7. Nanoconfined environments in intercalated (A) and exfoliated brush (B) systems. The outlined area schematically represents the regions where nanoconfinement occurs.

have been determined and compared for both nanocomposites (exfoliated and intercalated) and for virgin PS. Figure 4 shows that the glass transition temperature increases with increasing frequency. The frequency dependence of the glass transition temperature is plotted in Figure 5. The slopes of ln f vs $1/T_g$ plots yield the averaged values of E for the glass transition. It is seen that both nanocomposites demonstrate larger value of E than virgin PS. An increase in E relative to the respective value for virgin PS reveals the effect of nanoconfinement of PS chains in the nanocomposites. This supports the conjecture that nanoconfinement in both PS−clay materials enhances intermolecular interaction so that the polymer chains encounter larger energy barrier to their motion. Needless to say, hindered molecular mobility suggests a decrease in chemical reactivity or an increase in stability of the nanocomposites. From the comparable values of E (Figure 5) for the 1% exfoliated clay system (605 kJ mol^{-1}) and the 5% intercalated clay system (591 kJ mol^{-1}), it can be expected that these two systems experience a similar level of nanoconfinement. On the other hand, the intercalated PS−clay system with 1% of clay demonstrates the E value of 511 kJ mol^{-1} (not shown in Figure 5) that is reflective of a lower extent of nanoconfinement. This suggests that the formation of the brush structure via the SIP method can be a more efficient way of confining and stabilizing a polymer matrix.

By analyzing the quasi-static heat capacity, $C_{p,0}$ (Figure 6), one can evaluate the size of cooperatively rearranging regions according to the Donth equation (eq 8). The application of this equation to the $C_{p,0}$ data for the exfoliated PS−clay brush material and virgin PS reference shows that the PS−clay brush has a significantly larger V_{CRR} value of (64.5 ± 1.4 nm^3) than that of virgin PS (27.4 ± 4.8 nm^3). This is consistent with the previous result[30] obtained by regular DSC on the same materials. Similar analysis has been carried out for the intercalated PS−clay materials. Surprisingly, the resulting values of V_{CRR} have not shown any significant increase compared to the value for virgin PS. Even for a 5% clay load the size of a cooperatively rearranging region in the intercalated nanocomposite is 29.9 ± 4.6 nm^3 which is practically the same value as in virgin PS (27.4 ± 4.8 nm^3). By its meaning[47,48] the cube root of V_{CRR} represents the average distance between the mobility islands in the heterogeneous structure of an amorphous polymer. In other words, V_{CRR} provides a spatial measure of the dense regions that would include the nanoconfined regions in the present PS−clay systems. Therefore, the fact that V_{CRR} increases significantly in the exfoliated brush material and does not practically change in the intercalated system indicates an important difference in the structure of the bulk polymer in the respective nanoconfined environments (Figure 7). In the brush material, the nanoconfinement of polymer chains spreads from the clay surface throughout the length of the bristles of the brush. As a result, a significant volume of the bulk polymer experiences nanoconfinement that is reflected in the increasing volume of the cooperatively rearranging region. Apparently, this does not occur in the intercalated material because nanoconfinement is localized primarily within the narrow interfacial region near the clay surface, as suggested by the aforementioned simulation studies.[61−64]

Conclusions

Nanoconfinement of PS chains affects dramatically their dynamics which causes significant alterations in physical and chemical behavior of the nanocomposites as compared to virgin PS. Enhanced intermolecular interaction increases the probability of interchain reactions that is revealed as a high yield of α-methylstyrene in the degradation products of the two structurally different (intercalated versus exfoliated) PS−clay nanocomposites studied in this work. Comparative kinetic analysis of the degradation and relaxation processes in the nanocomposites also shows that nanoconfinement reveals itself in such physical parameters as the activation energy of the glass transition, the activation energy of the thermal degradation, and the size of cooperatively rearranging region. Of these three parameters, the activation energies of the glass transition and of degradation appear to be independent of the type of nanoconfinement because in both nanocomposites these values consistently demonstrate an increase as compared to the respective values for virgin PS. Since the activation energy of the glass transition tends to increase with increasing the clay load in the intercalated system, this parameter may be of relevance for estimating the extent of nanoconfinement and ultimately building structure property relationships for nanocomposites. On the other hand, the size of the cooperatively rearranging region is clearly structure dependent, because compared to virgin PS its value shows a significant increase in the exfoliated PS−clay brush material but practically no change in the intercalated PS−clay system. Therefore, this parameter can be useful in characterizing the structure of nanoconfinement. The invariability of its value for a nanocomposite as compared to that for a regular nonconfined polymer matrix indicates that nanoconfinement is localized at the clay particles. However, a significant increase in the size of cooperatively rearranging region suggests that nanoconfinement is more delocalized throughout the polymer matrix.

The terminology of barrier formation has been commonly used to describe the enhanced thermal and fire stability of polymer−clay nanocomposites. However, nanoconfinement appears to present a more specific description of the phenomenon which is responsible for this effect so the usage of this term is strongly encouraged. As the authors envision the process, polymer degradation starts and the newly formed radicals are nanoconfined, permitting a variety of bimolecular reactions to occur. As degradation progresses, the clay platelets, driven by a decrease in the surface free energy,[10] migrate gradually to the surface and form the barrier that has been detected by XPS.[9] This barrier is not the factor which prevents mass transport and offers thermal protection in the early stages of degradation but is rather something which occurs after the nanoconfinement. The latter is the significant event that controls the early stages of degradation and, therefore, contributes to the enhancement of the thermal and fire stability of polymer−clay nanocomposites.

Acknowledgment. The authors thank Dr. Xiaowu Fan for providing a sample of exfoliated PS−clay nanocomposites, and Dr. Tim Fulghum (University of Houston) for performing SEC analyses. Thanks are also due to Mettler-Toledo Inc. for donating the TGA instrument and loaning multifrequency temperature-modulated DSC (TOPEM).

References and Notes

(1) Alexandre, M.; Dubois, P. *Mater. Sci. Eng. R* **2000**, *28*, 1.
(2) Ray, S. S.; Okamoto, M. *Prog. Polym. Sci.* **2003**, *28*, 1539.
(3) Okada, A.; Usuki, A. *Macromol. Mater. Eng.* **2006**, *291*, 1449.
(4) Leszczynska, A.; Njuguna, J.; Pielichowski, K.; Banerjee, J. R. *Thermochim. Acta* **2007**, *453*, 75.
(5) Leszczynska, A.; Njuguna, J.; Pielichowski, K.; Banerjee, J. R. *Thermochim. Acta* **2007**, *454*, 1.
(6) Bourbigot, S.; Duquesne, S. *J. Mater. Chem.* **2007**, *17*, 2283.
(7) Gilman, J. W. *Appl. Clay Sci.* **1999**, *15*, 31.
(8) Gilman, J. W.; Jackson, C. L.; Morgan, A. B.; Harris, R.; Manias, E.; Giannelis, E. P.; Wuthenow, M.; Hilton, D.; Phillips, S. H. *Chem. Mater.* **2000**, *12*, 1866.
(9) Wang, J.; Du, J.; Zhu, J.; Wilkie, C. A. *Polym. Degrad. Stab.* **2002**, *77*, 249.
(10) Lewin, M. *Fire Mater.* **2003**, *27*, 1.
(11) Zanetti, M.; Bracco, P.; Costa, L. *Polym. Degrad. Stab.* **2004**, *85*, 657.
(12) Zanetti, M.; Camino, G.; Reichert, P.; Mulhaupt, R. *Macromol. Rapid Comm.* **2001**, *22*, 176.
(13) Zhu, J.; Uhl, F. M.; Morgan, A. B.; Wilkie, C. A. *Chem. Mater.* **2001**, *13*, 4649.
(14) Shen, Z.; Simon, G. P.; Cheng, Y.-B. *J. Appl. Polym. Sci.* **2004**, *92*, 2101.
(15) Lu, H.; Nutt, S. *Macromolecules* **2003**, *36*, 4010.
(16) Bandi, S.; Schiraldi, D. A. *Macromolecules* **2006**, *39*, 6537.
(17) Chen, J.; Poliks, M. D.; Ober, C. K.; Zhang, Y.; Wiesner, U.; Giannelis, E. *Polymer* **2002**, *43*, 4895.
(18) Lee, Y. H.; Bur, A. J.; Roth, S. C.; Start, P. R. *Macromolecules* **2005**, *38*, 3828.
(19) Bohning, M.; Goering, H.; Fritz, A.; Brzezinka, K. W.; Turky, G.; Schonhals, A.; Schartel, B. *Macromolecules* **2005**, *38*, 2764.
(20) Zhao, J.; Morgan, A. B.; Harris, J. D. *Polymer* **2005**, *46*, 8641.
(21) Nyden, M. R.; Gilman, J. W. *Comput. Theor. Polym. Sci.* **1997**, *7*, 191.
(22) Krishnamoorti, R.; Vaia, R. A. *Polymer nanocomposites: synthesis, characterization, and modeling*; American Chemical Society: Washington, DC, 2002.
(23) Giannelis, E. P.; Krishnamoorti, R.; Manias, E. Polymer-silicate nanocomposites: Model systems for confined polymers and polymer brushes. In *Polymers In Confined Environments*; Springer: Berlin, 1999; Vol. 138; pp 107.
(24) Auerbach, S. M.; Carrado, K. A.; Dutta, P. K. *Handbook of layered materials*; M. Dekker: New York, 2004.
(25) Rothon, R. N. *Particulate-filled Polymer Composites*, 2nd ed.; Rapra Technology Limited: Shawbury, U.K., 2003.
(26) Chen, K.; Susner, M. A.; Vyazovkin, S. *Macromol. Rapid Comm.* **2005**, *26*, 690.
(27) Chen, K.; Vyazovkin, S. *Macromol. Chem. Phys.* **2006**, *207*, 587.
(28) Vyazovkin, S.; Dranca, I.; Fan, X. W.; Advincula, R. *Macromol. Rapid Comm.* **2004**, *25*, 498.
(29) Vyazovkin, S.; Dranca, I.; Fan, X. W.; Advincula, R. *J. Phys. Chem. B* **2004**, *108*, 11672.
(30) Vyazovkin, S.; Dranca, I. *J. Phys. Chem. B* **2004**, *108*, 11981.
(31) Guyot, A. *Polym. Degrad. Stab.* **1986**, *15*, 219.
(32) McNeill, I. C.; Zulfiqar, M.; Kousar, T. *Polym. Degrad. Stab.* **1990**, *28*, 131.
(33) Kruse, T. M.; Woo, O. S.; Wong, H. W.; Khan, S. S.; Broadbelt, L. J. *Macromolecules* **2002**, *35*, 7830.
(34) Jang, B. N.; Wilkie, C. A. *Polymer* **2005**, *46*, 2933.
(35) Schawe, J. E. K.; Hutter, T.; Heitz, C.; Alig, I.; Lellinger, D. *Thermochim. Acta* **2006**, *446*, 147.
(36) Zhu, J.; Wilkie, C. A. *Polym. Int.* **2000**, *49*, 1158.
(37) Fan, X.; Xia, C.; Advincula, R. C. *Colloid Surf. A-Physicochem. Eng. Asp.* **2003**, *219*, 75.
(38) Fan, X.; Xia, C.; Fulghum, T.; Park, M. K.; Locklin, J.; Advincula, R. C. *Langmuir* **2003**, *19*, 916.
(39) Flynn, J. H. *Encyclopedia of polymer science and engineering*; Wiley: New York, 1989; Vol. Suppl.
(40) Vyazovkin, S.; Sbirrazzuoli, N. *Macromol. Rapid Comm.* **2006**, *27*, 1515.
(41) Vyazovkin, S. *J. Comput. Chem.* **1997**, *18*, 393.
(42) Vyazovkin, S. *J. Comput. Chem.* **2001**, *22*, 178.
(43) Flynn, J. H.; Wall, L. A. *J. Polym. Sci. B-Polym. Lett.* **1966**, *4*, 323.
(44) Ozawa, T. *Bull. Chem. Soc. Jpn.* **1965**, *38*, 1881.
(45) Strobl, G. R. *The physics of polymers: concepts for understanding their structures and behavior*, 2nd ed.; Springer: Berlin, 1997.
(46) Moynihan, C. T.; Easteal, A. J.; Wilder, J.; Tucker, J. *J. Phys. Chem.* **1974**, *78*, 2673.
(47) Donth, E. J. *The glass transition: relaxation dynamics in liquids and disordered materials*; Springer: Berlin, 2001.
(48) Donth, E. *J. Polym. Sci. B: Polym. Phys.* **1996**, *34*, 2881.
(49) *Polymer handbook*; 3rd ed.; Brandrup, J., Immergut, E. H., Eds.; Wiley: New York, 1989.

(50) Hempel, E.; Hempel, G.; Hensel, A.; Schick, C.; Donth, E. *J. Phys. Chem. B* **2000**, *104*, 2460.

(51) Qiu, L.; Chen, W.; Qu, B. *Polymer* **2006**, *47*, 922.

(52) Kandare, E.; Deng, H.; Wang, D.; Hossenlopp, J. M. *Polym. Advan. Technol.* **2006**, *17*, 312.

(53) Avella, M.; Carfagna, C.; Cerruti, P.; Errico, M. E.; Gentile, G. *Macromol. Symp.* **2006**, *234*, 163.

(54) Jost, W. *Diffusion in solids, liquids, gases*; Academic Press: New York, 1960.

(55) Gilman, J. W.; Jr., R. H. H.; Shields, J. R.; Kashiwagi, T.; Morgan, A. B. *Polym. Adv. Technol.* **2006**, *17*, 263.

(56) Vyazovkin, S. *Int. J. Chem. Kinet.* **1996**, *28*, 95.

(57) Vaia, R. A. Structural Characterization of Polymer-Layered Silicate Nanocomposites. In *Polymer-Clay Nanocomposites*; Pinnavaia, T. J., Beall, G. W., Eds.; Wiley: New York, 2000.

(58) Vermogen, A.; Masenelli-Varlot, K.; Seguela, R.; Duchet-Rumeau, J.; Boucard, S.; Prele, P. *Macromolecules* **2005**, *38*, 9661.

(59) Vaia, R. A.; Liu, W.; Koerner, H. *J. Polym. Sci. B: Polym. Phys.* **2003**, *41*, 3214.

(60) Százdi, L.; Ábrányi, Á.; Jr., B. P.; Vancso, J. G.; Pukánszky, B. *Macromol. Mater. Eng.* **2006**, *291*, 858.

(61) Starr, F. W.; Schroder, T. B.; Glotzer, S. C. *Macromolecules* **2002**, *35*, 4481.

(62) Zhang, Q.; Archer, L. A. *J. Chem. Phys.* **2004**, *121*, 10814.

(63) Daoulas, K. C.; Harmandaris, V. A.; Mavrantzas, V. G. *Macromolecules* **2005**, *38*, 5780.

(64) Smith, K. A.; Vladkov, M.; Barrat, J. L. *Macromolecules* **2005**, *38*, 571.